Defining the early stages of intestinal colonisation by whipworms

María A. Duque-Correa[a,*], David Goulding[a], Claire Cormie[a,1], Catherine Sharpe[b,2], Judit Gali Moya[c], Caroline Ridley[b], Catherine McCarthy[a], Kelly S. Hayes[b], Allison J. Bancroft[b], Claudia M Carneiro[d], Tobias Starborg[b], David J. Thornton[b], Richard K. Grencis[b,^], Matthew Berriman[a,^]

[a]Wellcome Sanger Institute, Wellcome Genome Campus, Hinxton, CB10 1SA, UK.

[b]Lydia Becker Institute of Immunology and Inflammation, Wellcome Trust Centre for Cell Matrix Research and Faculty of Biology, Medicine and Health, University of Manchester, Manchester, M13 9PT, UK.

[c]Faculty of Biology, University of Barcelona, Barcelona, 08028, Spain.

[d]Immunopathology Laboratory, NUPEB, Federal University of Ouro Preto, Campus Universitario Morro do Cruzeiro, Ouro Preto, MG, 35400-000, Brazil.

[1]Current Address: Cambridge Institute of Therapeutic Immunology and Infectious Disease, University of Cambridge, CB2 0AW, UK.

[2]Current Address: InstilBio, UMIC Bio-Incubator, Manchester, M13 9XX, UK.

^These authors contributed equally to this work.

[*]**Corresponding author. E-mail:** md19@sanger.ac.uk

ABSTRACT

Hundreds of millions of people are infected with whipworms *(Trichuris trichiura)*, large metazoan parasites that live in the caecum and proximal colon. Whipworms inhabit distinct multi-intracellular epithelial burrows that have been described as syncytial tunnels. However, the interactions between first-stage (L1) larvae and the host epithelia that determine parasite invasion and establishment in the syncytium remain unclear. *In vivo* experiments investigating these events have been severely hampered by the limited *in situ* accessibility to intracellular infective larvae at the bottom of the crypts of Lieberkühn, and the lack of genetic tools such as fluorescent organisms that are readily available for other pathogens but not parasitic nematodes. Moreover, cell lines, which do not mimic the complexity of the intestinal epithelium, have been unsuccessful in supporting infection by whipworm larvae. Here, we show that caecaloids grown in an open crypt-like conformation recapitulate the caecal epithelium. Using this system, we establish *in vitro* infections with *T. muris* L1 larvae for the first-time, and provide clear evidence that syncytial tunnels are formed at this early stage. We show that larval whipworms are completely intracellular but woven through multiple cells. Using the caecaloids, we are able to visualise the pathways taken by the larvae as they burrow through the epithelial cells. We also demonstrate that larvae degrade the mucus layers overlaying the epithelium, enabling them to access the cells below. We show that early syncytial tunnels are composed of enterocytes and goblet cells that are alive and actively interacting with the larvae during the first 24 h of the infection. Progression of infection results in damage to host cells and by 72 h post-infection, we show that desmosomes of cells from infected epithelium widen and some host cells appear to become liquified. Collectively, our work unravels processes mediating the intestinal epithelium

invasion by whipworms and reveals new specific interactions between the host and the parasite that allow the whipworm to establish on its multi-intracellular niche. Our study demonstrates that caecaloids can be used as a relevant *in vitro* model to investigate the infection biology of *T. muris* during the early colonisation of its host.

INTRODUCTION

Whipworms *(Trichuris spp)* are large metazoan parasites infecting a broad range of vertebrate hosts including humans, pigs, dogs and mice. Human whipworms *(T. trichiura)* infect hundreds of millions of people and cause trichuriasis, a major Neglected Tropical Disease[1,2]. Whipworm infections cause high chronic morbidity with dire socio-economic consequences in affected countries[2,3]. There are no vaccines to prevent infection and current chemotherapy is inefficient in achieving complete deworming[1,2]. A deeper mechanistic understanding of whipworm interactions with their host cells will enable the design of novel tools to fight the disease[1].

Whipworms live in the caecum and proximal colon of their hosts and have a unique life cycle strategy where they establish a multi-intracellular niche within intestinal epithelial cells (IECs)[4-6]. In this niche, whipworms can remain for years causing chronic infections[1,2]. *T. trichiura* is experimentally intractable, but a mouse model of infection with the natural rodent-infecting species *T. muris* closely mirrors infections in humans[4]. Most current knowledge on the biology of whipworm infections has been provided by the *T. muris* model[4].

Infection with whipworms follows ingestion of eggs from the external environment[1,2,4]. Upon arrival in the caecum and proximal colon, eggs hatch in a process mediated by the host microbiota[4,7] *(Fig 1A)*. Within hours, motile first stage (L1) larvae (100-150 μm long) released from the eggs enter the intestinal epithelia (IE) at the bottom of the crypts of Lieberkühn, where stem cells reside[5,8-10] *(Fig 1A)*. To reach this location, L1 larvae need to overcome barriers that protect the stem cell niche. Specifically, larvae have to transverse the mucus layer, which is thickest at the crypt openings, enter through small crypt openings (around 6 μm) and then move

against the continuous stream of fluid that flushes from the crypt to the lumen[11]. To date, the physical and molecular cues directing the larvae to this location and mediating their penetration through the overlying mucus into the IE are unknown.

To accommodate themselves completely inside the IE, the larvae burrow through several IECs creating multinucleated cytoplasmic masses, that result from the fusion of adjacent cell membranes but are bordered apically, laterally and basally by IEC membranes, and have been described as syncytial tunnels[12]. The earliest that syncytial tunnels have been detected from the L3 larval stage (around day 21 post infection (p.i.)), when they become visible on the surface of the IE[6,12]. The syncytium is thought to provide a sheltered environment and a continuous source of nutrients that is extended by the worm when exhausted and as it moults four times to reach adulthood[6,12-14]. Inside the syncytium the worm is in direct contact with the cytoplasm and organelles of the IECs[6,12]. The biology and the mechanisms of formation of the multicellular epithelial tunnels are unknown[1]. During the first days of infection, whether the IECs forming the tunnels are dead, or alive and interacting with the parasite and orchestrating the development of immune responses remains controversial[6,12,15,16]. Moreover, the strategies used by whipworms to colonise this habitat and adapt to its physical-chemical conditions remain unidentified.

Investigations on IEC interactions with whipworms mediating invasion and establishment of syncytial tunnels have been severely hampered by the limited *in situ* accessibility to intracellular larvae *in vivo*, which infect IECs at the bottom of the crypts that account for less than 1% of the caecal epithelium, and the lack of genetic tools to generate fluorescent larvae. Moreover, an *in vitro* culture system to study early infection events is not available because cell lines do not support infection by whipworm L1 larvae.

Intestinal organoids are *in vitro* multicellular clusters that closely recapitulate IE architecture and the full complement of stem and differentiated cell types[17-19]. Intestinal organoids have been successfully used to model mouse and human IE responses to a variety of viral, bacterial and protozoan pathogens[18,20-23]. While organoids have recently been used to study interactions of IECs with excretory/secretory molecules produced by helminths, they have not yet been exploited to study direct interactions between host IE and live helminths[24,25]. In the present study, we have used murine caecaloids[25] grown in an open crypt-like conformation, to establish *in vitro* infection with *T. muris* L1 larvae for the first-time, effectively reproducing whipworm infection *in vivo*. This novel system enabled us visualise the syncytium in its entirety and to investigate the cellular and molecular processes mediating larvae invasion of the IE and establishment within multicellular epithelial tunnels during the first three days of infection. Our results provide a clear view of the structure of early syncytial tunnels, including evidence of close host IE-whipworm interactions occurring during whipworm colonisation of their niche. We demonstrate that the caecaloid-*T. muris* larvae system represents a physiologically relevant *in vitro* model to investigate the events defining early whipworm infection of its host.

MATERIALS AND METHODS

Mice

Wild-type (WT) C57BL/6N mice were kept under specific pathogen-free conditions, and colony sentinels tested negative for *Helicobacter* spp. Mice were fed a regular autoclaved chow diet (LabDiet) and had *ad libitum* access to food and water. All efforts were made to minimize suffering by considerate housing and husbandry. Animal welfare was assessed routinely for all mice involved. Mice were naïve prior the studies here described.

Ethics Statement

The care and use of mice were in accordance with the UK Home Office regulations (UK Animals Scientific Procedures Act 1986) under the Project licenses 80/2596 and P77E8A062 and were approved by the institutional Animal Welfare and Ethical Review Body.

Parasites and *T. muris* infection

Infection and maintenance of *T. muris* was conducted as described[26]. Age and sex matched female WT mice (6–10-week-old) were orally infected under anaesthesia with isoflurane with a high (400) dose of embryonated eggs from *T. muris* E-isolate. Mice were randomised into uninfected and infected groups using the Graph Pad Prism randomization tool. Uninfected and infected mice were co-housed. Mice were monitored daily for general condition and weight loss. Mice were culled including concomitant uninfected controls at different time points. Mice were killed by cervical dislocation and caecum and proximal colon were collected for downstream processing. Blinding at the point of measurement was achieved by the use of

barcodes. During sample collection, group membership could be seen, however this stage was completed by technician staff with no knowledge of the experiment objectives.

3D Caecaloid culture

Mouse 3D caecaloids lines from C57BL/6N adult mice (6-8 weeks old) were derived from caecal epithelial crypts as previously described[25]. Briefly, the caecum was cut open longitudinally and luminal contents removed. Tissue was then minced, segments were washed with ice cold Dulbecco's PBS1X without calcium and magnesium (PBS) (Gibco Thermo Fisher Scientific) and vigorous shaking to remove mucus, and treated with Gentle Cell Dissociation Reagent (STEMCELL Tech) for 15 min at room temperature (RT) with continuous rocking. Released crypts were collected by centrifugation, washed with ice cold PBS, resuspended in 200 µl of cold Matrigel (Corning), plated in 6-well tissue culture plates and overlaid with a Wnt rich medium containing base growth medium (Advanced DMEM/F12 with 2 mM Glutamine, 10 mM HEPES, 1X penicillin/streptomycin, 1X B27 supplement, 1X N2 supplement (all from Gibco Thermo Fisher Scientific)), 50% Wnt3a conditioned medium (Wnt3a cell line, kindly provided by the Clevers laboratory, Utrecht University, Netherlands), 10% R-spondin1 conditioned medium (293T-HA-Rspo1-Fc cell line, Trevigen), 1 mM N-acetylcysteine (Sigma-Aldrich), 50 ng/ml rmEGF (Gibco Thermo Fisher Scientific), 100 ng/ml rmNoggin (Peprotech), 100 ng/ml rhFGF-10 (Peprotech) and 10 µM Rho kinase (ROCK) inhibitor (Y-27632) dihydrochloride monohydrate (Sigma-Aldrich). Caecaloids were cultured at 37ºC, 5% CO_2. The medium was changed every two days and after one week, Wnt3a conditioned medium was reduced to 30% and penicillin/streptomycin was removed (expansion medium). Expanding caecaloids were passaged, after recovering from Matrigel using

ice-cold PBS or Cell Recovery Solution (Corning), by physical dissociation through vigorous pipetting with a p200 pipette every six to seven days.

Caecaloid culture in 2D conformation using transwells

3D caecaloids grown in expansion medium for 4-5 days after passaging were dissociated into single cells by TrypLE Express (Gibco Thermo Fisher Scientific) digestion. 200,000 cells in 200 µl base growth medium were seeded onto 12 mm transwells with polycarbonate porous membranes of 0.4 µm (Corning) pre-coated with 50 mg/ml rat tail collagen I (Gibco Thermo Fisher Scientific). Cells were cultured with expansion medium in the basolateral compartment for two days. Then, basolateral medium was replaced with medium containing 10% Wnt3a conditioned medium for additional 48 h. To induce differentiation of cultures, medium in the apical compartment was replaced with 50 µl base growth medium and medium in the basolateral compartment with medium containing 2.5% Wnt3A conditioned medium that was changed every two days. Cultures were completely differentiated when cells pumped the media from the apical compartment and cultures looked dry.

In vitro* hatching of *T. muris* eggs with *Escherichia coli

E. coli K-12 was grown in Luria Bertani broth overnight at 37ºC and shaking at 200rpm. Eggs were added to bacterial cultures and incubated for 2 h at 37ºC, 5% CO_2. Larvae were washed with PBS three times to remove *E. coli* by centrifugation at 720 *g* for 10 min at RT. Bacteria was killed by culturing larvae in RPMI 1640 (Gibco Thermo Fisher Scientific), 10% Foetal Bovine Serum (FBS) (Gibco Thermo Fisher Scientific), 2 mM L-glutamine (Sigma-Aldrich), 1X antibiotic/antimycotic (Sigma Aldrich) and 1 mg/ml ampicillin (Roche) for 2 h at 37ºC, 5% CO_2. Larvae were washed with RPMI 1640 three times to remove ampicillin and separated from

egg shells and unembryonated eggs using a step 50-60% Percoll (Sigma Aldrich) gradient. Centrifugation at 300 *g* for 15 min at RT was performed and the 50% interface layer was collected. Recovered larvae were washed with RPMI 1640 and resuspended in media containing Primocin (InvivoGen).

T. muris L1 larvae infection of caecaloids grown in transwells

Differentiated caecaloid cultures in transwells were infected with 300 L1 *T. muris* larvae obtained by *in vitro* hatching of eggs in presence of *E. coli*. Larvae in a volume of 100 µl of base growth medium were added to the apical compartment of the transwells. Infections were maintained for up to 72 h at 37ºC, 5% CO_2.

Immunofluorescence (IF) staining

For IF, caecaloid cultures in transwells were fixed with 4% Formaldehyde, Methanol-free (Thermo Fisher) in PBS for 20 min at 4ºC, washed three times with PBS and permeabilized with 2% Triton X-100 (Sigma-Aldrich) 5% FBS in PBS for 1 h at RT. Caecaloids were then incubated with primary antibodies α-villin (1:100, Abcam, ab130751), α-Ki-67 (1:250, Abcam, ab16667), α-chromogranin A (1:50, Abcam, ab15160), α-Dcamlk-1 (1:200, Abcam, ab31704), α-zona occludens-1 (ZO-1) protein (1:200, Invitrogen, 61-7300) and the lectins *Ulex europaeus* agglutinin - Atto488 conjugated (UEA, 1:100, Sigma-Aldrich, 19337) and *Sambucus nigra* - Fluorescein conjugated (SNA, 1:50, Vector Laboratories, FL-1301) diluted in 0.25% Triton X-100 5% FBS in PBS overnight at 4ºC. After three washes with PBS, caecaloids were stained with secondary antibody Donkey anti-rabbit IgG Alexa Fluor 555 (1:400, Molecular Probes, A31572), phalloidin Alexa Fluor 647 (1:1000, Life Technologies, A22287) and 4',6'-diamidino-2-phenylindole (DAPI, 1:1000, AppliChem, A1001.0010) at RT for 1 h. Transwell membranes were washed three times with PBS and

mounted on slides using ProLong Gold anti-fade reagent (Life Technologies Thermo Fisher Scientific). Confocal microscopy images were taken with a Leica SP8 confocal microscope and processed using the Leica Application Suite X (LAS X) software.

Cell death fluorescence staining

To evaluate cell death in infected caecaloids, cultures were incubated with 100 µl warm base growth medium containing 0.3 mg/ml of propidium iodide (Sigma-Aldrich) and 8 µM of CellEvent™ Caspase-3/7 Green Detection Reagent (Invitrogen) for 30 min at 37ºC 5% CO2. Then, caecaloids were fixed and counterstained as described above.

Transmission electron microscopy (EM)

Tissues and caecaloids were fixed in 2.5% glutaraldehyde/2% paraformaldehyde in 0.1M sodium cacodylate buffer, post-fixed with 1% osmium tetroxide and mordanted with 1% tannic acid followed by dehydration through an ethanol series (contrasting with uranyl acetate at the 30% stage) and embedding with an Epoxy Resin Kit (all from Sigma-Aldrich). Semi-thin 0.5µm sections were cut and collected onto clean glass slides and dried at 60°C before staining with 1% Toluidine Blue and 1% Borax (all from Sigma-Aldrich) in distilled water for 30 seconds. Sections were then rinsed in distilled water and mounted in DPX (Sigma-Aldrich) and coverslipped. Sections were imaged on a Zeiss 200M Axiovert microscope.

Ultrathin sections cut on a Leica UC6 ultramicrotome were contrasted with uranyl acetate and lead nitrate, and images recorded on a FEI 120 kV Spirit Biotwin microscope on an F416 Tietz CCD camera.

Scanning EM

Caecaloids were fixed with 2.5% glutaraldehyde and 4% paraformaldehyde in 0.01 M PBS at 4°C for 1 h, rinsed thoroughly in 0.1 M sodium cacodylate buffer three times, and fixed again in 1% buffered osmium tetroxide for 3 h at RT. To improve conductivity, using the protocol devised by Malick and Wilson[27], the samples were then impregnated with 1% aqueous thiocarbohydrazide and osmium tetroxide layers, with the steps separated by sodium cacodylate washes. They were then dehydrated three times using an ethanol series (30, 50, 70, 90, and 100% ethanol, 20 min each) before they were critical point dried in a Leica EM CPD300 and mounted on aluminium stubs with conducting araldite and sputter coated with a 2-nm platinum layer in a Leica EM ACE 600. Images were taken on a HITACHI SU8030.

Serial block face scanning EM

Samples from caecum of infected mice were processed according to Deerinck et al[28]. Embedded tissues were mounted and serial sectioned on a Gatan 3View System and simultaneously imaged on a Zeiss Merlin SEM. Serial images were oriented and assimilated into corrected z-stacks using IMOD. The phenotype of infected cells was determined in each image and number cells of each cellular population were quantified.

Mucin 2 (MUC2) and caecaloid mucus degradation experiments

Glycosylated MUC2 was derived from LS174T cells, purified as previously described[29] and incubated with 400 *T. muris* L1 larvae for 24 h at 37ºC, 5% CO_2. For experiments with caecaloid cultures, after 72 h of L1 larvae infection, mucus was recovered by three PBS washes followed by six washes with 0.2 M urea.

Rate zonal centrifugation

Mucus degradation analysis was conducted as described[29]. Briefly, purified MUC2 (in 4 M guanidinium chloride (GuCl)) was loaded onto the top of 6–8 M GuCl gradients and centrifuged in a Beckman Optima L-90K Ultracentrifuge (Beckman SW40 rotor) at 40,000 RPM for 2.75 h 15ºC. Alternatively, mucus samples (in PBS or 0.2 M urea) were loaded onto 5-25% (w/v) linear sucrose gradients and centrifuged in a Beckman Optima L-90K Ultracentrifuge (Beckman SW40 rotor) at 40,000 RPM for 3 h 15ºC. After centrifugation tubes were emptied from the top and the fractions probed with a MUC2 antibody or using the Periodic Acid Shiff (PAS) assay. To determine the sucrose or GuCl concentration the refractive index of each fraction was measured using a refractometer; all sucrose and GuCl gradients were comparable (data not shown).

QUANTIFICATION AND STATISTICAL ANALYSIS

Desmosome separation measurements in uninfected, distant to worm and adjacent (infected) cells in caecaloids were compared using Kruskal Wallis and Dunn's comparison tests from the Prism 8.2 software (GraphPad). Statistical comparison for *in vivo* uninfected and infected mice and the *in vitro* and *in vivo* models was done using Mann-Whitney tests from the Prism 8.2 software (GraphPad).

RESULTS

Caecaloids, an *in vitro* model mimicking *T. muris* L1 larvae infection of enterocytes and goblet cells at the bottom of the crypts of Lieberkühn

Light microscopy studies dating back 40-50 years have shown *T. muris* L1 larvae infecting cells at the base of the crypts of Lieberkühn in the first hours p.i.[5,8,9]. Confirming these findings, we found L1 larvae invading IECs at crypt bases of the caecum and proximal colon of *T. muris*-infected mice as early as three hours p.i. *(Fig 1B; Supplementary Fig 1A-C).* Except for the presence of worms within the IECs, little else could be discerned about the nature of the host-parasite interactions using light microscopy. However, TEM revealed L1 larvae infecting enterocytes and goblet cells *(Fig 1C)*. Our observations were often limited to histological sections with a transverse view through a single slice of the worm within an IEC. Indeed, due to the intricate topography of the multicellular epithelial tunnels the larvae burrow through, it has proved very challenging to obtain longitudinal sections of the complete worm inside its niche. Therefore, we next used serial block face SEM, which allowed us to capture the entire syncytial tunnel formed by two L1 larvae *(Supplementary video 1 and 2)* and revealed that by this three-hour time point, larvae were completely intracellular. A detailed analysis of the individual images led us to identify and quantify the type of infected IECs. We observed that a typical syncytial tunnel was composed of approximately 40 IECs, with 75% of those cells being enterocytes and 15% goblet cells *(Supplementary Fig 1D)*. While illuminating, this technically demanding and expensive approach is, importantly, constrained to finding L1 larvae in the tissue, which is very challenging due to their intracellular location of at the bottom of the crypts and the small ratio of infected IECs in the total caecal epithelia.

Hence, to further examine the processes of invasion and formation of the syncytial tunnels, we required an *in vitro* system to directly dissect the interactions between infected IECs and the parasite at the early whipworm mucosal niche. To date, epithelial cell lines have been used unsuccessfully to recreate IE infection by whipworms, probably because they lack the cellular and architectural complexity of the IE[24]. Thus, a first step towards an *in vitro* model for whipworm infection was to establish a three-dimensional (3D) organoid culture recapitulating the complexity of the mouse caecal epithelium. We recently developed protocols to grow and differentiate caecaloids containing all IECs populations present in the caecal epithelium[25]. We successfully microinjected *T. muris* L1 larvae into the lumen of caecaloids but the larvae did not invade the IECs and after 24 h stopped moving and appeared to be dead. These experiments suggested that the physicochemical conditions required to promote L1 larvae invasion and survival could not be recreated within the caecaloid lumen. In a second approach, we adapted protocols[30-32] to culture organoids in an open conformation using Transwells. Specifically, 3D caecaloids were dissociated into single cells and cultured in Transwell membranes *(Fig 1D)*. The basolateral compartment of the Transwell contained Wnt3a conditioned medium at sequentially reduced concentrations and cells in the apical compartment were exposed to a semi-wet interface to stimulate IEC differentiation. These culture conditions promoted the generation of self-organizing structures with a specific configuration of stem, goblet, tuft, absorptive and enteroendocrine cells that resembled crypts present in the caecum *(Supplementary Fig 2A-G).* Besides providing unique access to all IEC populations, this culture-system featured a mucus layer overlaying the IECs and polarized microvilli *(Supplementary Fig 2H and I).* L1 larvae were obtained by hatching *T. muris* eggs in the presence of *E. coli,* to

simulate microbiota exposure[7] and the Transwell system allowed the L1 larvae to be directly cultured with the IECs *(Fig 1D)*.

To address whether *T. muris* L1 larvae invaded the caecaloids grown in transwells, we first performed confocal microscopy after 24 h of co-culture. We observed L1 larvae infecting IECs as evidenced by enterocyte microvilli (villin) staining above the worm *(Fig 1E)* and z-stack confocal images showing the larvae woven through multiple IECs *(Fig 1F)*. Next, we ruled out the possibility that the larvae had simply dislodged the IECs rather than actually penetrated the cells. We captured invasion of goblet cells by L1 larvae with SEM *(Fig 1G)* and by TEM we found larvae within the cytoplasm of enterocytes and goblet cells *(Fig 1H).* Together, these images show L1 larvae infecting IECs for the first time *in vitro,* effectively reproducing *in vivo* infection. The caecaloids model enabled the entirety of the L1 larva and its host cells to be visualised. Moreover, our results suggest that close interactions of absorptive and goblet cells with L1 larvae are critical during invasion and colonisation of the IE by whipworms.

Fig 1. Caecaloid - *T. muris* L1 larvae *in vitro* model reproduces whipworm *in vivo* infection

A. Illustration of the processes of egg hatching at the caecal lumen and larvae infection of the IE at the base of the crypts. **B.** Images of toluidine blue-stained transverse sections from caecum of WT mice infected with *T. muris* (3 and 72 h p.i.), showing whipworm larvae (arrowhead) infecting cells at the base of crypts. Scale bar 30μm. **C.** TEM images of transverse sections from caecum of WT mice infected with *T. muris,* showing whipworm L1 larvae infecting goblet cells **(I and III)** and enterocytes **(II)** at 3 h p.i. Scale bar 5μm. Blue lines show the cellular membranes of

the host cells. **D.** Scheme of the caecaloid-whipworm model experimental set-up. **E and F.** Confocal IF images of caecaloids infected with whipworm L1 larvae for 24 h. **E.** Orthogonal slice visualising enterocyte microvilli (villin staining in red) above the larvae (arrowheads). Scale bar 20µm. **F.** Complete z stack projection and selected and cropped volume showing larvae infecting different IECs. In red, **(I)** Dclk-1, marker of tuft cells; **(II)** Ki-67, marker of proliferating cells, stem and TA cells. In green, the lectins UEA and SNA bind mucins in goblet cells; in blue and aqua, DAPI stains nuclei of IECs and larvae, respectively; and in white, Phalloidin binds to F-actin. Scale bar 20µm. **G.** Scanning and **F.** Transmission EM images from caecaloids infected with *T. muris* for 24 h, showing whipworm L1 larvae within enterocytes and goblet cells. Blue lines show the cellular membranes of the host cells.

Supplementary Fig 1. Whipworm L1 larvae infects IE at the bottom of the crypts of Lieberkühn in the caecum

A-C. Images of toluidine blue-stained transverse sections from caecum of WT mice infected with *T. muris* at 3 h p.i., showing whipworm larvae (arrowhead) infecting cells at the base of crypts. **D.** Numbers of enterocytes and goblet cells infected by whipworm L1 larvae in syncytial tunnels *in vivo* (24 h p.i.). Counts on serial block face SEM images of two syncytial tunnels. Points are the counts for each individual worm.

Supplementary Fig 2. Characterisation of caecaloids grown in transwells

Images of caecaloids grown and differentiated in transwells showing the presence of all IEC populations organized in structures resembling intestinal crypts. **A-D.**

Confocal IF microscopy with antibodies staining **(A)** Ki-67, marker of proliferating cells, stem and TA cells; **(B)** Villin, identifying microvilli of enterocytes; **(C)** Chromogranin A expressing enteroendocrine cells; **(D)** Dclk-1, marker of tuft cells; **(A-D)** and with the lectins UEA and SNA that bind mucins in goblet cells. DAPI stains nuclei and Phalloidin binds to F-actin. Scale bar 100µm for A and B, 50µm for C and D. **E-F**. Transmission EM showing goblet and enteroendocrine cells **(E)** and enterocytes **(F).** Scanning EM showing mucus and goblet cells **(H)**, microvilli of enterocytes **(I)** and tuft cells **(G)**.

Whipworm L1 larvae invade the caecal epithelium by degrading the overlaying mucus layer

After hatching and to counter host peristalsis, whipworm L1 larvae rapidly reach the bottom of the crypt and invade the IECs[9]. But first, the larvae must traverse the outer and inner mucus layers overlaying the IE. Despite whipworm larvae motility, mucus can aggregate around them, blocking their advance towards the IE; therefore, an additional mechanism is required for larvae to transverse the mucus layers. Many intestinal pathogens have evolved enzymes to degrade the mucin oligosaccharides via glycosidases, exposing the mucin peptide backbone to proteases[33]. Proteolytic cleavage of mucins causes disassembly of the polymerized mucin network, reducing mucus viscosity, increasing its porosity and likely impairing mucus barrier function[29,33]. The protozoan parasite *Entamoeba histolytica* cleaves MUC2, the major component of intestinal mucus, breaking down the mucus network and facilitating invasion of the IECs[34]. Adult *T. muris* also degrades MUC2 via secretion of serine proteases[29]. Thus, we hypothesised that secretion of proteases by L1 larvae results

in degradation of the overlaying mucus layer. To test this hypothesis, we first determined whether L1 larvae have a direct effect on MUC2 by exposing purified glycosylated MUC2 to L1 larvae for 24 h at 37ºC. L1 larvae treated and untreated (control) MUC2 samples were subjected to rate-zonal centrifugation to ascertain the size distribution of the mucins. After exposure to L1 larvae, MUC2 had an altered sedimentation profile, with a higher proportion of slower sedimenting mucins (between fractions 1-8) indicating a reduction in mucin size due to depolymerization *(Fig 2A)*. Next, we evaluated changes in the mucus layer of caecaloids upon L1 larvae infection. Light microscopy of Toluidine blue-stained transverse sections of infected caecaloids showed that the mucus layer immediately overlaying larvae-infected IECs was less densely stained than the mucus overlaying neighbouring uninfected regions and uninfected caecaloids *(Fig 2B)*, again indicating degradation. We then recovered mucus from L1 larvae-infected and uninfected caecaloids after 72 h and examined the mucin size distribution by using rate-zonal centrifugation. Consistent with our results from purified MUC2, we again observed an altered sedimentation profile with a shift in the distribution to a lower sedimentation rate in infected samples demonstrating degradation of mucin polymers *(Fig 2C)*.

Collectively, these data suggest that degradation of mucus by L1 larvae enables whipworms to penetrate through the mucus layer and invade the underlying IECs.

Fig 2. Whipworm L1 larvae invades caecal epithelium by degrading the overlaying mucus layer

A. MUC2 purified from LS174T cell lysates was incubated with or without 400 L1 larvae at 37^{o}C for 24 h before being subjected to rate zonal centrifugation on linear 6-8M GuHCl gradients. After centrifugation tubes were emptied from the top and the

fractions probed with a MUC2 antibody; data are shown as staining intensity arbitrary units (a. u). Results are represented as the mean +/-Standard Error of the Mean (SEM) of 3 independent experiments. Black circles: untreated, red squares: treated with whipworm L1 larvae. **B.** Representative images of a toluidine blue-stained transverse sections from caecaloids uninfected and infected with *T. muris* for 24 h showing degradation (asterisk) of the overlaying mucus layer immediate above the infected cells. Scale bar 20µm. **C.** Caecaloid mucus degradation by L1 larvae after 72 h p.i. Transwells were washed with PBS and urea 0.2M to recover mucus. Washes were subjected to rate zonal centrifugation on linear 5-25% sucrose gradients. After centrifugation tubes were emptied from the top and the fractions were stained with PAS; data are shown as staining intensity arbitrary units (a. u). Results are represented as the mean +/- SEM of 3 replicas of one independent experiment. Black circles: untreated, red squares: treated with whipworm L1 larvae.

Close interactions between *T. muris* L1 larvae and IECs defining the whipworm niche in the syncytial tunnels

After crossing the mucus layer, the L1 larva becomes intracellular creating a syncytium, a hallmark of whipworm infections *(Fig 1)*. Only previously described for later larval and adult stages[6,12], syncytial tunnels are suggested to form by lateral burrowing of whipworms through adjacent IECs that join to form a single structure housing the parasite. Presently, the process of formation of the tunnels is not understood. Using our caecaloid system to recreate early events of an *in vivo* infection, we examined the host-parasite interactions of the L1 larvae and the IECs composing the syncytial tunnels. The intricate path of the tunnels formed by L1 larvae burrowing through IECs was revealed by confocal IF microscopy of infected

caecaloids *(Figs 3A and B, Supplementary videos 3 and 4).* Tilney *et al.* previously observed that the syncytium around the anterior end of L3-L4 larvae and adult worms is an inert scaffold of dead cells with a brush border cover[6]. In contrast, staining with propidium iodide, to mark necrotic cells, and caspase 3/7, to label apoptotic cells, revealed that while cells left behind in the tunnel were dead, the IECs actively infected by the worm were in fact alive *(Fig 3C).*

To better characterise interactions between the host IECs and the larvae inside the tunnels, we performed TEM on *T. muris*-infected caeca and caecaloids during the first 72 h of infection. As early as 3 h p.i. of mice and 24 h p.i in caecaloids, we observed larvae in direct contact with the IECs cytoplasm as no cell membrane could be seen between the whipworm cuticle and the cytoplasm *(Figs 1C* and *H, 4)*. During their transit path, larvae displaced cellular organelles *(Figs 1C* and *H, 4)* and burrowed through mucin secretory granules of goblet cells, possibly causing mucus discharge *(Fig 4A)*. Tannic acid staining revealed complex carbohydrate in the immediate vicinity surrounding the larvae, both between host cells and in bordering host cell cytoplasm, most likely secreted by the worm *(Fig 4A).* Electron micrographs at 3 h p.i. of mice showed the reorganization of the cytoskeleton of infected cells around the worm *(Fig 4B inset I).* This interaction was recreated at 24 h of caecaloid infection where we also found deposition of the actin fibres of IECs surrounding the worm cuticle *(Fig 4D, inset I).* Several host cell nuclei are found in the tunnels containing the worms *(Figs 3, 4C-E, 5A, C* and *D),* and with infection progression chromatin is visibly condensed and fragmenting indicating onset of apoptosis *(Figs 4C* and *E*, *5C* and *D)*. Host cells in the caecum and caecaloids have numerous mitochondria, which are displaced by the larvae *(Figs 4B inset II, C* and *E inset I, 5C inset II)*. At 72 h p.i of caecaloids, several lysosomes are found in infected cells,

many of which are being discharged over the larvae cuticle *(Fig 4E insets II and III).* Taken together, these findings suggest that early in an infection there is an active interplay between the IECs and the parasite at its multi-intracellular niche that may shape the initial host responses to the larvae.

Fig 3. Intricate path of syncytial tunnels burrowed by whipworm L1 larvae revealed in caecaloids

A-B. Complete z stack projection and selected and cropped volume of confocal IF images of syncytial tunnels (arrowheads) in caecaloids infected with L1 whipworm larvae for 24 h. In red, **(A)** Dclk-1, marker of tuft cells; **(B)** ZO-1 protein, binding tight junctions; in green, the lectins UEA and SNA bind mucins in goblet cells; in blue and aqua, DAPI stains nuclei of IECs and larvae, respectively; and in white, Phalloidin binds to F-actin. Scales bar for **(A)** 50μm, for inset 20μm, and **(B)** 20μm. **C.** Selected confocal IF 2D images from a z-stack showing IECs left behind in the tunnel are necrotic (propidium iodide and caspase 3/7 positive), while IECs infected by worm are alive after 72h p.i. Scale bar 50μm.

Fig 4. Close interactions between *T. muris* whipworm larvae and IECs at syncytial tunnels during early infection

TEM images of transverse sections from caecum of mice and caecaloids infected with *T. muris* L1 larvae, showing host-parasite interactions during early infection. **A-B.** Larvae infecting goblet cells in the caecum of mice 3 h p.i., note **(A)** potential mucus discharge (white arrowhead) and tannic acid staining revealing complex carbohydrate in the host cell cytoplasm and between cells (inset, red arrow); **(B)** host cell cytoskeleton (actin) reorganization around the cuticle of the larvae (inset I) and

displacement of host cell mitochondria by the worm (inset II). **C-E.** Larvae infecting several IECs in the caecum of mice and caecaloids at 24 and 72 h p.i. **(C, E)** Host cells display DNA condensation and fragmentation (characteristic for the onset of apoptosis) and numerous mitochondria. **(D)** Host cell actin fibres surround the cuticle of the worm (inset I) and desmosomes (red asterisks) are still present (inset II). **(E)** Host cells present numerous lysosomes, some actively discharging over the worm cuticle (insets II and III). N, nuclei.

Whipworm burrowing through IECs ultimately results in tissue damage

IE barrier integrity is maintained by intercellular junctions between the IECs including, from apical to basal, tight junctions, adherens junctions, and desmosomes[35,36]. Syncytial tunnels hosting stage 3 and 4 larvae and adult whipworms present an intact apical surface stabilised by the actin cytoskeleton and cell junctions and a basal surface that remains attached to the basement membrane, but lateral membranes of the host IECs are ruptured[6]. We therefore searched for a similar effect at our much earlier stage of the infection and evaluated intercellular junctions on the syncytial tunnels on infected caeca and caecaloids using confocal microscopy and TEM. Lateral membranes of host cells are still visible and separating their cytoplasm *(Figs 1C* and *H)* and staining with an antibody binding ZO-1 protein in caecaloids shows tight junctions are still present on infected cells, but have disappeared in the cells left behind in the tunnel *(Fig 3B* and *Supplementary Fig 3A and video 5).* While all intercellular junctions are still present in infected cells after 72 h of infection *(Supplementary Fig 3B)*, desmosomes, but not tight and adherens junctions, appeared to be separated *(Figs 5A* and *B, Supplementary Fig 3B)*. Thus,

we measured desmosome separation between infected and adjacent cells, cells 1 mm distant from the worm (in caecaloids only) and uninfected cells. Desmosomes joining infected IECs and adjacent cells have opened *(Figs 5A* and *B)*. When compared to those of uninfected cells, the distance between desmosomes joining infected IECs and adjacent cells significantly increased from 26 nm to 38 nm *(Figs 5A* and *B)*. Strikingly, we observed equivalent perturbations *in vitro* and *in vivo (Supplementary Fig 3C)*, further demonstrating that the caecaloid-whipworm model closely recapitulates whipworm infection.

With infection progression, at 72 h p.i., we also detected other alterations in infected IECs of both caecaloids and caecum of infected mice, including cell liquefaction and pyknotic nuclei indicating early apoptosis *(Fig 5C* and D*)*. Altogether, our results indicate that with progression of infection, the tunnelling of the larvae across the IECs results in IECs damage.

Fig 5. Desmosome perturbations, cell liquefaction and early apoptotic nuclei in host cells of whipworm larvae during early infection.

A-B. Desmosome separation was measured on cells from caecaloids and caecum of WT mice infected with *T. muris* for 72 h and uninfected controls*.* **A.** Representative TEM images of transverse sections of infected caecaloids and desmosomes (arrowheads) joining infected and adjacent cells (I and II), cells 1mm distant to the worm from infected caecaloids (III), and cells from uninfected caecaloids. Scale bars for desmosome images 100nm. Desmosome separation in nm was measured in host cells from two independent worms. Adjacent and distant measurements n=37, uninfected measurements n=25. ***p<0.001 Kruskal Wallis and Dunn's comparison tests. **B.** Representative TEM images of transverse sections of caecum (scale bar

3µm) and desmosomes (arrowheads) joining infected and adjacent cells from infected mice and cells from uninfected mice. Scale bars for desmosome images 100nm. Desmosome separation in nm was measured in host cells from one worm. Adjacent measurements n=25, uninfected measurements n=25. **p<0.0025 Mann-Whitney test. **C.** Representative TEM images of transverse sections of infected caecaloids (72 h p.i.) showing liquefied cell (I, asterisk), mitochondria and nuclei in early stages of apoptosis (II). **D.** Toluidine blue-stained (scale bar 20µm) and TEM images of transverse sections from caecum of WT mice infected with *T. muris*, showing a syncytial tunnel formed by L1 whipworm larvae through IECs (72 h p.i.) and depicting liquefaction of cells (I, asterisk) and nuclei in early stages of apoptosis (II). N, nuclei.

Supplementary Fig 3. Perturbation of host cell desmosomes, but not tight and adherens junctions, upon whipworm L1 larvae infection

A. Complete z stack projections of confocal IF images of larva in syncytial tunnel in caecaloids infected with L1 whipworm larvae for 24h. In red, ZO-1 protein, binding tight junctions; in green, the lectins UEA and SNA bind mucins in goblet cells; in blue and aqua, DAPI stains nuclei of IECs and larvae, respectively; and in white, Phalloidin binds to F-actin. Scale bar 10µm. **B.** Representative TEM images of infected caecum after 72 h of infection showing intact tight and adherens junctions (white stars) but separated desmosomes (red stars) on cells hosting the larva. **D.** Representative TEM images of desmosomes from uninfected and infected caecaloids and caecum of mice. Scale bars 100nm. Statistical comparison between the desmosome separation measurements show no difference between the *in vitro* and *in vivo* models. n=25. Mann-Whitney test.

DISCUSSION

While the sequence of events in the very early phase of intestinal invasion and colonisation by whipworms are obvious targets for designing novel tools to prevent and treat *T. trichiura* infections, in the last 40 years almost no progress has been made in understanding this aspect of whipworm biology. A major drawback to these studies is the lack on an *in vitro* model reproducing early whipworm infections, which are difficult to investigate *in vivo* due to challenges in finding and accessing intracellular larvae at the bottom of the crypts of Lieberkühn, and the lack of genetic tools to generate fluorescent larvae. To overcome these limitations, in this study, we developed an *in vitro* model of infection with *T. muris* using caecaloids[25]; the first *in vitro* model to reproduce whipworm *in vivo* infections. Exploiting this system, together with *in vivo* observations where possible, interactions have been revealed between *T. muris* L1 larvae and IECs mediating whipworm penetration of the caecal epithelium and formation of syncytial tunnels through the first three days of infection.

Whipworm larvae infection is not supported by epithelial cell lines or 3D caecaloids indicating that complex interactions of the larvae with particular cellular or molecular components of the caecal epithelium and specific physicochemical conditions are critical in triggering parasite invasion. We now show that caecaloids grown and differentiated in an open conformation on transwells feature all caecal IEC populations, organised in crypt-like structures with tight centres of proliferating cells surrounded by differentiated cells, polarised microvilli and an overlaying mucus layer, thus recapitulating the complexity of the composition and architecture of the caecal epithelium. This system allows the direct culture of *T. muris* L1 larvae, which become intracellular during the first 24 h of infection. Of note, undifferentiated caecaloids, forming a complete monolayer but lacking differentiated cell types, do not support

larvae infection. These observations suggest that the cues and receptors sensed by the parasite to invade the IECs at the bottom of the crypts *in vivo* are replicated in differentiated caecaloids grown in transwells. Further research is needed to understand the nature of those molecular interactions.

Our caecaloid-whipworm larvae model enables us to study the processes of invasion and formation of syncytial tunnels to a level unattainable before, thus answering questions that cannot be otherwise investigated in the mouse model. To start, we examined how L1 larvae overcome the mucus barrier overlaying the IECs prior to invasion – experiments not possible *in vivo* due to the small ratio of larvae versus IECs in the caecum that would dilute the effects of the larvae on the mucus layer. Moreover, mucus produced by caecaloids better represents the complexity encountered by whipworm larvae than the much simpler purified MUC2 preparations commonly used *in vitro* experiments to assess mucus degradation. Using our *in vitro* system, we visualised mucus degradation *in situ* and detected depolymerisation of mucins upon larvae infection of caecaloids. These findings indicated that whipworm invasion of the IE is preceded by the degradation of the mucus layer by the parasite.

The complexity in terms of IECs populations and mucus layer present in the caecaloids grown in transwells will also enable critical investigations into the molecular mechanisms directing larvae movement towards and infection the IE at the crypt base. Other pathogens that preferentially colonise the large intestine such as *Shigella dysenteriae*[37] and *E. histolytica*[38,39] recognize tissue specific expression of mucin and mucin glycosylation patterns. *Trichuris* L1 larvae may also recognise molecular cues within the mucus to initiate invasion as Hasnain *et al* showed decreased establishment of *T. muris* in *Sat1*$^{-/-}$ mice with reduced sulphated mucus[40]. For penetration and tunnelling through IECs, expression of proteases by whipworm

L1 larvae may be critical as proteases secreted by other parasitic nematode infective larvae facilitate their entry in the intestinal wall of mammalian hosts[41,42]. Future studies using the caecaloid-whipworm larvae model together with live imaging tools to capture active invasion, and knock-out technologies and inhibitors, will determine the role of cellular and molecular components of both the IECs and larvae in whipworm colonisation of its niche.

The open conformation of the caecaloid system allowed us to visualise the syncytium entirely, and revealed its multi-intracellular composition and the intricate path of the tunnels created by the infective *T. muris* L1 larvae for the first time. Up to now, the syncytium was visibly recognizable as a tunnel only when L3 larvae reach the table of the crypts of the caecal or proximal colon epithelia and were large enough to cause a visible protrusion into the lumen[6,12]. Closely recapitulating *in vivo* *T. muris* infection, the early tunnels in the caecaloid model were composed by absorptive and goblet cells, which is in line with earlier observations indicating that these two cell types constitute the syncytium hosting older larval stages and adults[12]. Ascertaining the path of the L1 larvae inside the IE allowed us to discover that while the IECs ultimately succumb after the parasite has moved through them, when the larvae are within the IECs, they remain alive. Surprisingly, during the first 24 h of infection these host cells present minimal damage despite the presence of larva in direct contact with their cytoplasm, which has joined into a multinucleated mass yet conserving desmosomal contacts with adjacent cells and lateral membranes. We identified distinct host-parasite interactions in the tunnels including the reorganisation of the infected IECs cytoskeleton around the cuticle of the larvae suggesting a response of the host cell to the intracellular parasite. Moreover, we visualised a likely excretion/secretion of products by the larva into its immediate environment in the

cytoplasm of the infected IECs. These products may support its intracellular tunnelling by digesting the cells and/or block the activation of inflammatory responses by the IECs. We also detected numerous mitochondria in infected IECs when compared with uninfected neighbouring cells. Together these results revealed that the early syncytial tunnels are an interactive multi-intracellular niche where whipworms interact with their host cells potentially modifying their energy demands and metabolic activity.

With infection progression, at 72 h p.i., we detected in infected cells several lysosomes that surround and discharge over the cuticle of the larvae suggesting a direct response of the host cell to the parasite. In addition, we observed perturbations in IECs forming the syncytial tunnel including opening of the desmosomes, early pyknotic nuclei indicative of apoptosis and liquefaction of cells. These alterations replicated those observed *in vivo* and indicate that whipworm burrowing through IECs ultimately results in IE damage.

Similarities can be drawn between our observations in the early tunnels with those by Lee and Wright[12] on the thin anterior ends of L3-L4 larvae and adult worms that are intracellular and where cellular elements such as nuclei, lipid droplets, mitochondria, and mucous secretory granules can be identified. However, IECs in early syncytial tunnels display erect tall microvilli and lateral membranes, in contrast to those housing L3-L4 larvae and adult worms that have lost these features i.e. erect stature of the tunnel microvilli and where no lateral membranes are found to subdivide the cytoplasm surrounding the worm[6,12]. More distal to the head cellular elements become increasingly scarce and degenerated[12]. Lee and Wright[12] suggested that the worm induces a syncytium about its head, feeds on the syncytial

cytoplasm, and then moves on to initiate extension of the syncytium[12]. Our findings on the early syncytial tunnels support this hypothesis.

IE damage at the syncytial tunnels caused by the whipworm larvae either mechanically through tunnelling or chemically as induced by secretory/excretory products, potentially results in release of damage-associated molecular patterns (DAMPs) and alarmins by infected IECs, which have been suggested to initiate innate immune responses to the worm[15,16]. Because the caecaloid culture contains purely IECs, it offers a unique system to directly investigate how IECs respond to whipworm larvae, without mixing effects from other cellular populations present at the mucosa and submucosa of the caecum, such as stromal and immune cells. Future transcriptomic and proteomic studies on *T. muris* L1 larvae-infected caecaloids will reveal responses of both the worm and the IECs to infection and uncover host-parasite interactions critical for whipworm larvae invasion and colonisation of the caecal IE. Here, the caecaloid system will be critical to mechanistically define these interactions. Furthermore, the addition of stroma and immune cells to our *in vitro* system will allow us to elucidate the molecular mediators critical in the crosstalk between IECs and key cells from the stem cell niche that orchestrate the initiation of immune responses.

Our findings have unravelled early interactions between whipworm larvae and their host IECs that lead to the formation of syncytial tunnels and establishment of infection. We have demonstrated that caecaloids can be used as a relevant *in vitro* model to study the infection biology of *T. muris* during the early colonisation of its host. Extending the applicability of our caecaloid-whipworm system, adapting it to study *T. trichiura* L1 larvae infection of human caecal and proximal colon organoids will be an important next step. Further investigations on the early host-parasite

interplay within the whipworm mucosal niche will be fundamental to the development of new tools to help control trichuriasis and also provide novel insights into how the intestinal epithelium adapts to damage and mediates repair.

SUPPLEMENTARY VIDEOS

Supplementary videos 1 and 2. Visualisation of syncytial tunnels burrowed by *T. muris* L1 larvae infecting IECs *in vivo*. Videos visualising serial block face SEM images of syncytial tunnels in the caecum of *T. muris*-infected mice at 24 h p.i.

Supplementary Video 3. Visualisation of syncytial tunnel burrowed by *T. muris* L1 larva infecting IECs in caecaloids. Video visualising z-stack of confocal IF images of caecaloids infected with whipworm L1 larvae for 24 h. Note the intricate tunnel left behind by larva, which are completely multi-intracellular. Stained in blue are nuclei of both the epithelia cells and larvae (DAPI), in white is F-actin at cell membrane (phalloidin), in green are mucus vacuoles of goblet cells (UEA/SNA lectins binding mucin glycans) and in magenta are dividing cells (Ki-67).

Supplementary Video 4. Visualisation of syncytial tunnel burrowed by *T. muris* L1 larva infecting IECs in caecaloids. Video visualising z-stack of confocal IF images of caecaloids infected with whipworm L1 larvae for 24 h. Note the intricate tunnel left behind by larva, which are completely multi-intracellular. Stained in blue are nuclei of both the epithelia cells and larvae (DAPI), in white is F-actin at cell membrane (phalloidin), in green are mucus vacuoles of goblet cells (UEA/SNA lectins binding mucin glycans) and in red are tuft cells (Dckl-1).

Supplementary Video 5. Visualisation of tight junctions of host IECs from *T. muris* L1 larva in syncytial tunnel in caecaloids. Video visualising z-stack of confocal IF images of caecaloids infected with whipworm L1 larvae for 24 h. Note

tight junctions of infected IECs are conserved. Stained in blue are nuclei of both the epithelia cells and larvae (DAPI), in white is F-actin at cell membrane (phalloidin), in green are mucus vacuoles of goblet cells (UEA/SNA lectins binding mucin glycans) and in red are tight junctions (ZO-1 protein).

REFERENCES

1 Else, K. J. *et al.* Whipworm and roundworm infections. *Nat Rev Dis Primers* **6**, 44, doi:10.1038/s41572-020-0171-3 (2020).

2 Jourdan, P. M., Lamberton, P. H. L., Fenwick, A. & Addiss, D. G. Soil-transmitted helminth infections. *Lancet* **391**, 252-265, doi:10.1016/S0140-6736(17)31930-X (2018).

3 Pullan, R. L., Smith, J. L., Jasrasaria, R. & Brooker, S. J. Global numbers of infection and disease burden of soil transmitted helminth infections in 2010. *Parasit Vectors* **7**, 37, doi:10.1186/1756-3305-7-37 (2014).

4 Klementowicz, J. E., Travis, M. A. & Grencis, R. K. Trichuris muris: a model of gastrointestinal parasite infection. *Seminars in immunopathology* **34**, 815-828, doi:10.1007/s00281-012-0348-2 (2012).

5 Panesar, T. S. & Croll, N. A. The location of parasites within their hosts: site selection by Trichuris muris in the laboratory mouse. *Int J Parasitol* **10**, 261-273, doi:10.1016/0020-7519(80)90006-5 (1980).

6 Tilney, L. G., Connelly, P. S., Guild, G. M., Vranich, K. A. & Artis, D. Adaptation of a nematode parasite to living within the mammalian epithelium. *J Exp Zool A Comp Exp Biol* **303**, 927-945, doi:10.1002/jez.a.214 (2005).

7 Hayes, K. S. *et al.* Exploitation of the intestinal microflora by the parasitic nematode Trichuris muris. *Science* **328**, 1391-1394, doi:10.1126/science.1187703 (2010).

8 Wakelin, D. The development of the early larval stages of Trichuris muris in the albino laboratory mouse. *J Helminthol* **43**, 427-436, doi:10.1017/s0022149x00004995 (1969).

9 Panesar, T. S. The early phase of tissue invasion by Trichuris muris (nematoda: Trichuroidea). *Z Parasitenkd* **66**, 163-166, doi:10.1007/bf00925723 (1981).

10 Beer, R. J. Studies on the biology of the life-cycle of Trichuris suis Schrank, 1788. *Parasitology* **67**, 253-262, doi:10.1017/s0031182000046497 (1973).

11 Gehart, H. & Clevers, H. Tales from the crypt: new insights into intestinal stem cells. *Nat Rev Gastroenterol Hepatol* **16**, 19-34, doi:10.1038/s41575-018-0081-y (2019).

12 Lee, T. D. & Wright, K. A. The morphology of the attachment and probable feeding site of the nematode Trichuris muris (Schrank, 1788) Hall, 1916. *Can J Zool* **56**, 1889-1905, doi:10.1139/z78-258 (1978).

13 McKay, D. M., Shute, A. & Lopes, F. Helminths and intestinal barrier function. *Tissue Barriers* **5**, e1283385, doi:10.1080/21688370.2017.1283385 (2017).

14 O'Sullivan, J. D. B., Cruickshank, S. M., Starborg, T., Withers, P. J. & Else, K. J. Characterisation of cuticular inflation development and ultrastructure in Trichuris muris using correlative X-ray computed tomography and electron microscopy. *Sci Rep* **10**, 5846, doi:10.1038/s41598-020-61916-0 (2020).

15 Grencis, R. K. Immunity to helminths: resistance, regulation, and susceptibility to gastrointestinal nematodes. *Annu Rev Immunol* **33**, 201-225, doi:10.1146/annurev-immunol-032713-120218 (2015).

16 Artis, D. & Grencis, R. K. The intestinal epithelium: sensors to effectors in nematode infection. *Mucosal immunology* **1**, 252-264, doi:10.1038/mi.2008.21 (2008).

17 Date, S. & Sato, T. Mini-gut organoids: reconstitution of the stem cell niche. *Annu Rev Cell Dev Biol* **31**, 269-289, doi:10.1146/annurev-cellbio-100814-125218 (2015).
18 Fatehullah, A., Tan, S. H. & Barker, N. Organoids as an in vitro model of human development and disease. *Nat Cell Biol* **18**, 246-254, doi:10.1038/ncb3312 (2016).
19 Li, M. & Izpisua Belmonte, J. C. Organoids - Preclinical Models of Human Disease. *N Engl J Med* **380**, 569-579, doi:10.1056/NEJMra1806175 (2019).
20 Barrila, J. *et al.* Modeling Host-Pathogen Interactions in the Context of the Microenvironment: Three-Dimensional Cell Culture Comes of Age. *Infect Immun* **86**, doi:10.1128/IAI.00282-18 (2018).
21 Dutta, D. & Clevers, H. Organoid culture systems to study host-pathogen interactions. *Curr Opin Immunol* **48**, 15-22, doi:10.1016/j.coi.2017.07.012 (2017).
22 Dutta, D., Heo, I. & Clevers, H. Disease Modeling in Stem Cell-Derived 3D Organoid Systems. *Trends Mol Med* **23**, 393-410, doi:10.1016/j.molmed.2017.02.007 (2017).
23 In, J. G. *et al.* Human mini-guts: new insights into intestinal physiology and host-pathogen interactions. *Nat Rev Gastroenterol Hepatol* **13**, 633-642, doi:10.1038/nrgastro.2016.142 (2016).
24 Duque-Correa, M. A., Maizels, R. M., Grencis, R. K. & Berriman, M. Organoids - New Models for Host-Helminth Interactions. *Trends Parasitol* **36**, 170-181, doi:10.1016/j.pt.2019.10.013 (2020).
25 Duque-Correa MA., S. F., Rodgers FH, Goulding D, Forrest S, White R, Buck A, Grencis RK and Berriman M. Development of caecaloids to study host-pathogen interactions: new insights into immunoregulatory functions of Trichuris muris extracellular vesicles in the caecum. *bioRxiv*, doi:doi.org/10.1101/2020.05.11.087684 (2020).
26 Wakelin, D. Acquired immunity to Trichuris muris in the albino laboratory mouse. *Parasitology* **57**, 515-524 (1967).
27 Malick, L. E. & Wilson, R. B. Modified thiocarbohydrazide procedure for scanning electron microscopy: routine use for normal, pathological, or experimental tissues. *Stain Technol* **50**, 265-269, doi:10.3109/10520297509117069 (1975).
28 Deerinck, T. J., Bushong, E. A., Lev-Ram, V., Shu, X., Tsien, R.Y. and Ellisman, M. H. . Enhancing Serial Block-Face Scanning Electron Microscopy to Enable High Resolution 3-D Nanohistology of Cells and Tissues. *Microscopy and Microanalysis* **16** 1138-1139, doi:doi:10.1017/S1431927610055170 (2010).
29 Hasnain, S. Z., McGuckin, M. A., Grencis, R. K. & Thornton, D. J. Serine protease(s) secreted by the nematode Trichuris muris degrade the mucus barrier. *PLoS neglected tropical diseases* **6**, e1856, doi:10.1371/journal.pntd.0001856 (2012).
30 Moon, C., VanDussen, K. L., Miyoshi, H. & Stappenbeck, T. S. Development of a primary mouse intestinal epithelial cell monolayer culture system to evaluate factors that modulate IgA transcytosis. *Mucosal immunology* **7**, 818-828, doi:10.1038/mi.2013.98 (2014).
31 Navabi, N., McGuckin, M. A. & Linden, S. K. Gastrointestinal cell lines form polarized epithelia with an adherent mucus layer when cultured in semi-wet

interfaces with mechanical stimulation. *PLoS One* **8**, e68761, doi:10.1371/journal.pone.0068761 (2013).

32 Wang, X. *et al.* Cloning and variation of ground state intestinal stem cells. *Nature* **522**, 173-178, doi:10.1038/nature14484 (2015).

33 McGuckin, M. A., Linden, S. K., Sutton, P. & Florin, T. H. Mucin dynamics and enteric pathogens. *Nat Rev Microbiol* **9**, 265-278, doi:10.1038/nrmicro2538 (2011).

34 Lidell, M. E., Moncada, D. M., Chadee, K. & Hansson, G. C. Entamoeba histolytica cysteine proteases cleave the MUC2 mucin in its C-terminal domain and dissolve the protective colonic mucus gel. *Proc Natl Acad Sci U S A* **103**, 9298-9303, doi:10.1073/pnas.0600623103 (2006).

35 Buckley, A. & Turner, J. R. Cell Biology of Tight Junction Barrier Regulation and Mucosal Disease. *Cold Spring Harb Perspect Biol* **10**, doi:10.1101/cshperspect.a029314 (2018).

36 Luissint, A. C., Parkos, C. A. & Nusrat, A. Inflammation and the Intestinal Barrier: Leukocyte-Epithelial Cell Interactions, Cell Junction Remodeling, and Mucosal Repair. *Gastroenterology* **151**, 616-632, doi:10.1053/j.gastro.2016.07.008 (2016).

37 Sudha, P. S., Devaraj, H. & Devaraj, N. Adherence of Shigella dysenteriae 1 to human colonic mucin. *Curr Microbiol* **42**, 381-387, doi:10.1007/s002840010234 (2001).

38 Ravdin, J. I. & Guerrant, R. L. Role of adherence in cytopathogenic mechanisms of Entamoeba histolytica. Study with mammalian tissue culture cells and human erythrocytes. *J Clin Invest* **68**, 1305-1313, doi:10.1172/jci110377 (1981).

39 Chadee, K., Petri, W. A., Jr., Innes, D. J. & Ravdin, J. I. Rat and human colonic mucins bind to and inhibit adherence lectin of Entamoeba histolytica. *J Clin Invest* **80**, 1245-1254, doi:10.1172/JCI113199 (1987).

40 Hasnain, S. Z. *et al.* Immune-driven alterations in mucin sulphation is an important mediator of Trichuris muris helminth expulsion. *PLoS Pathog* **13**, e1006218, doi:10.1371/journal.ppat.1006218 (2017).

41 Tort, J., Brindley, P. J., Knox, D., Wolfe, K. H. & Dalton, J. P. Proteinases and associated genes of parasitic helminths. *Advances in parasitology* **43**, 161-266, doi:10.1016/s0065-308x(08)60243-2 (1999).

42 Dzik, J. M. Molecules released by helminth parasites involved in host colonization. *Acta Biochim Pol* **53**, 33-64 (2006).

Figure 1.

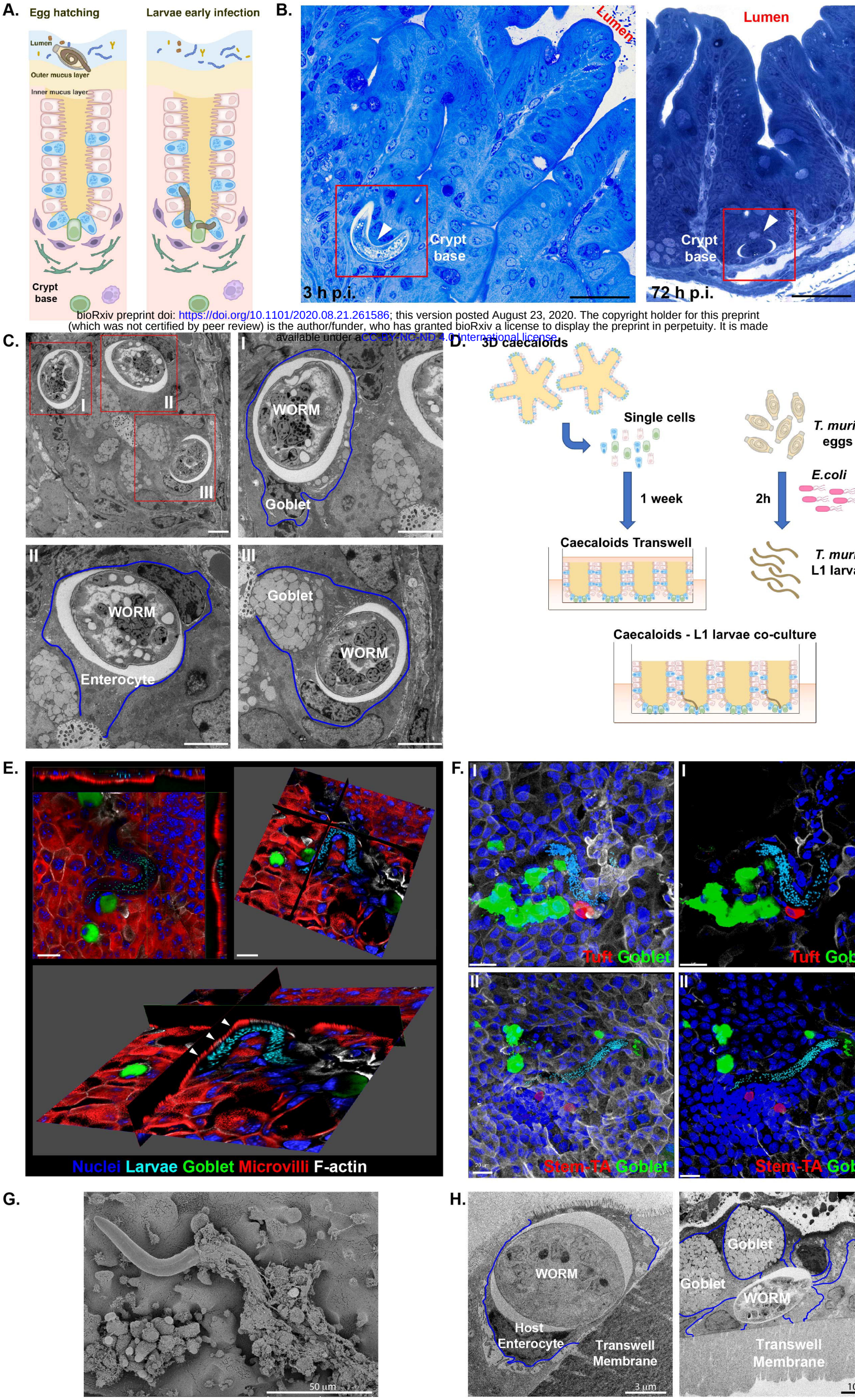

Figure 2.

A.

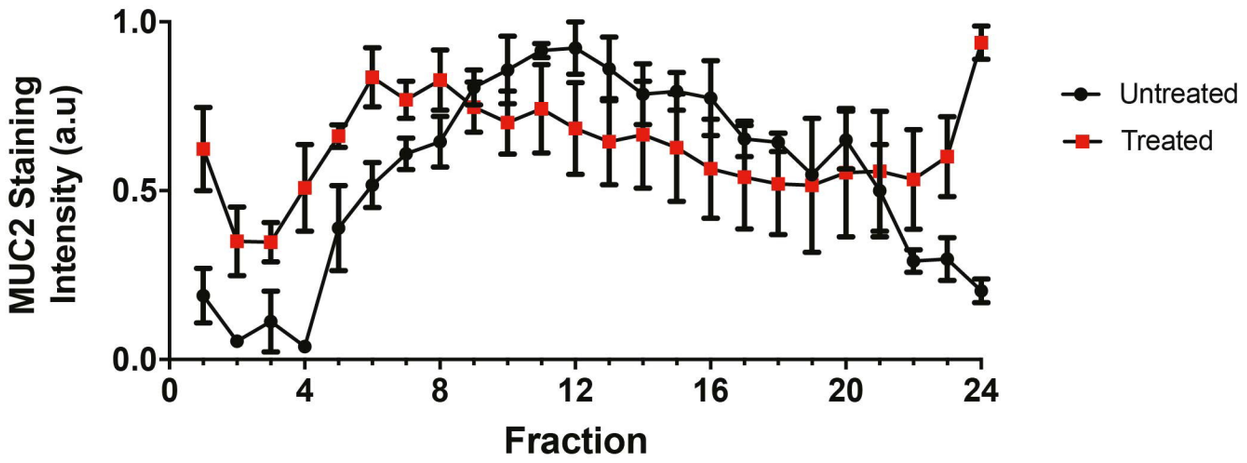
MUC2 Staining Intensity (a.u)
1.0
0.5
0.0
0
4
8
12
16
20
24
Fraction
Untreated
Treated

B.

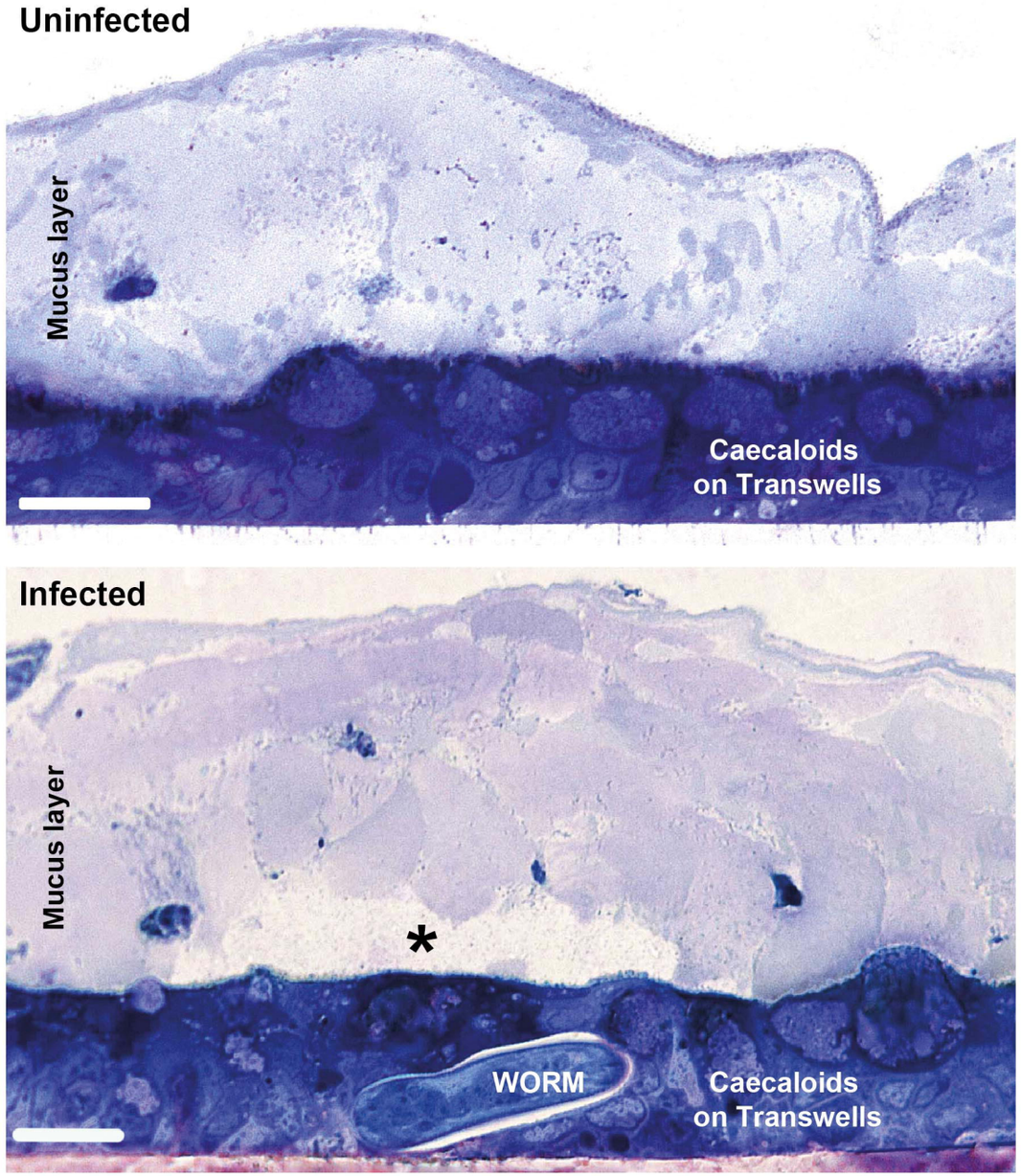
Uninfected
Mucus layer
Caecaloids on Transwells
Infected
Mucus layer
*
WORM
Caecaloids on Transwells

C.

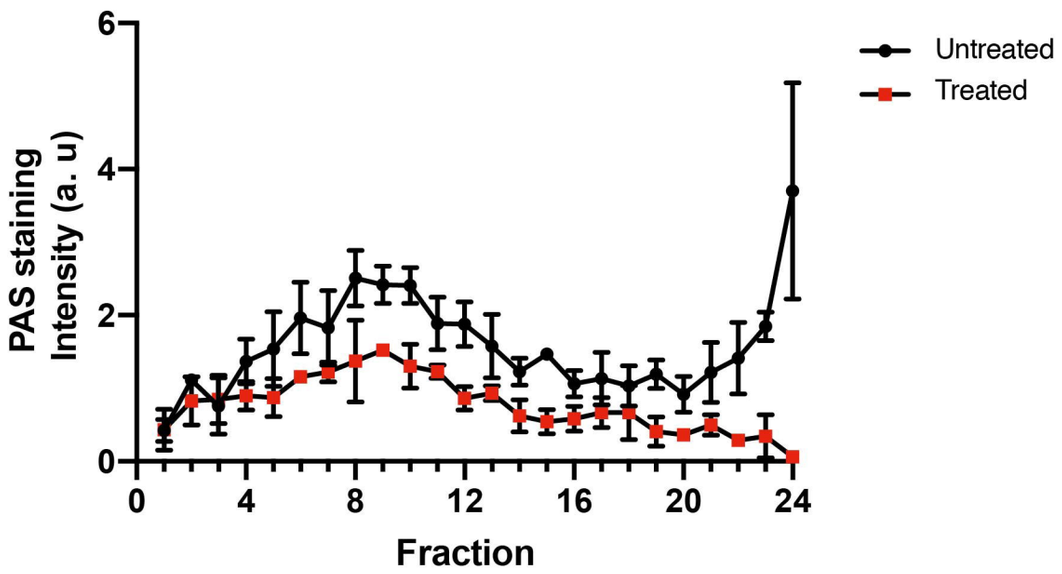
PAS staining Intensity (a. u)
6
4
2
0
0
4
8
12
16
20
24
Fraction
Untreated
Treated

Figure 3.

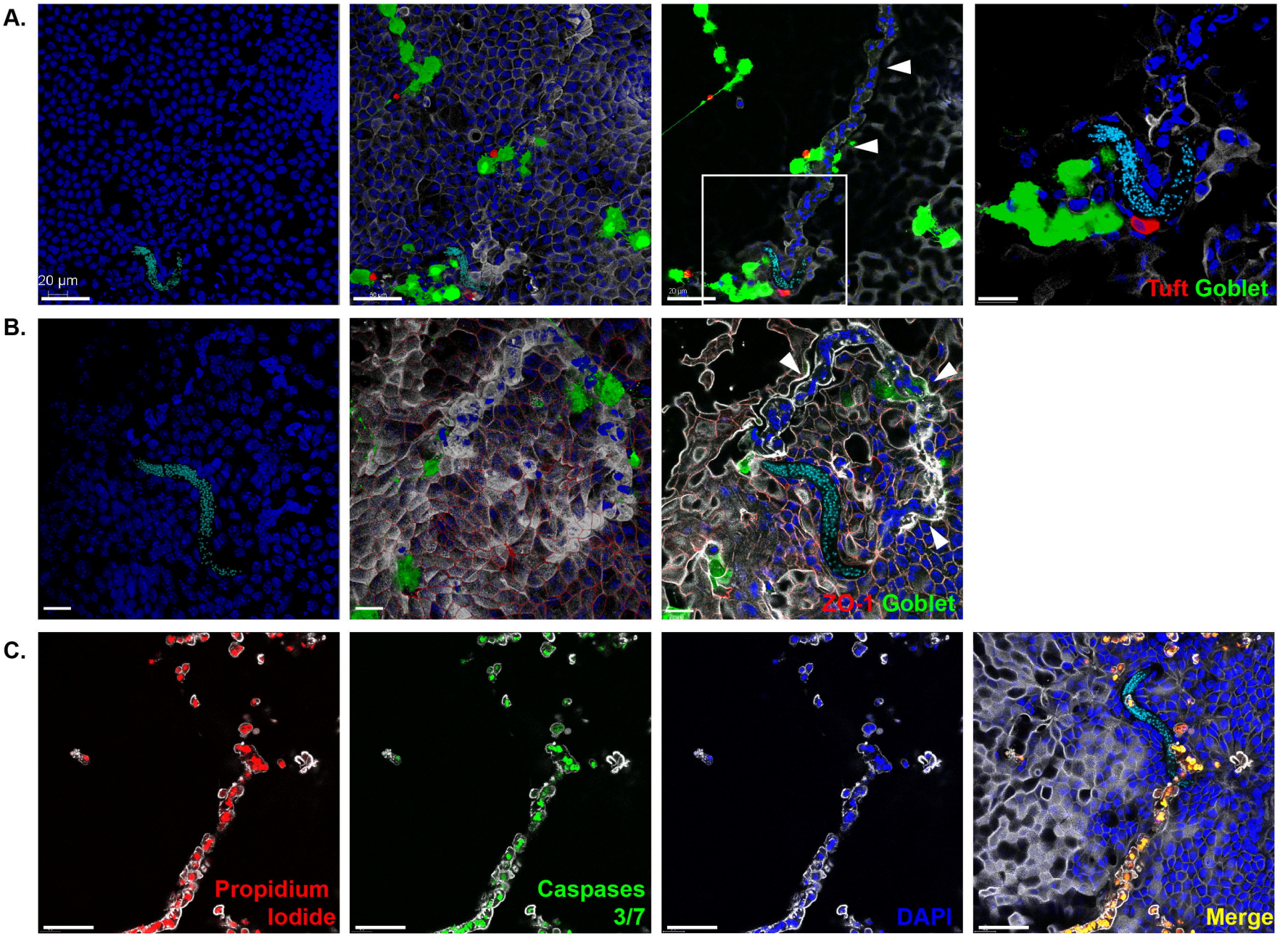
A.
20 µm
Tuft Goblet
B.
ZO-1 Goblet
C.
Propidium Iodide
Caspases 3/7
DAPI
Merge

Figure 4.

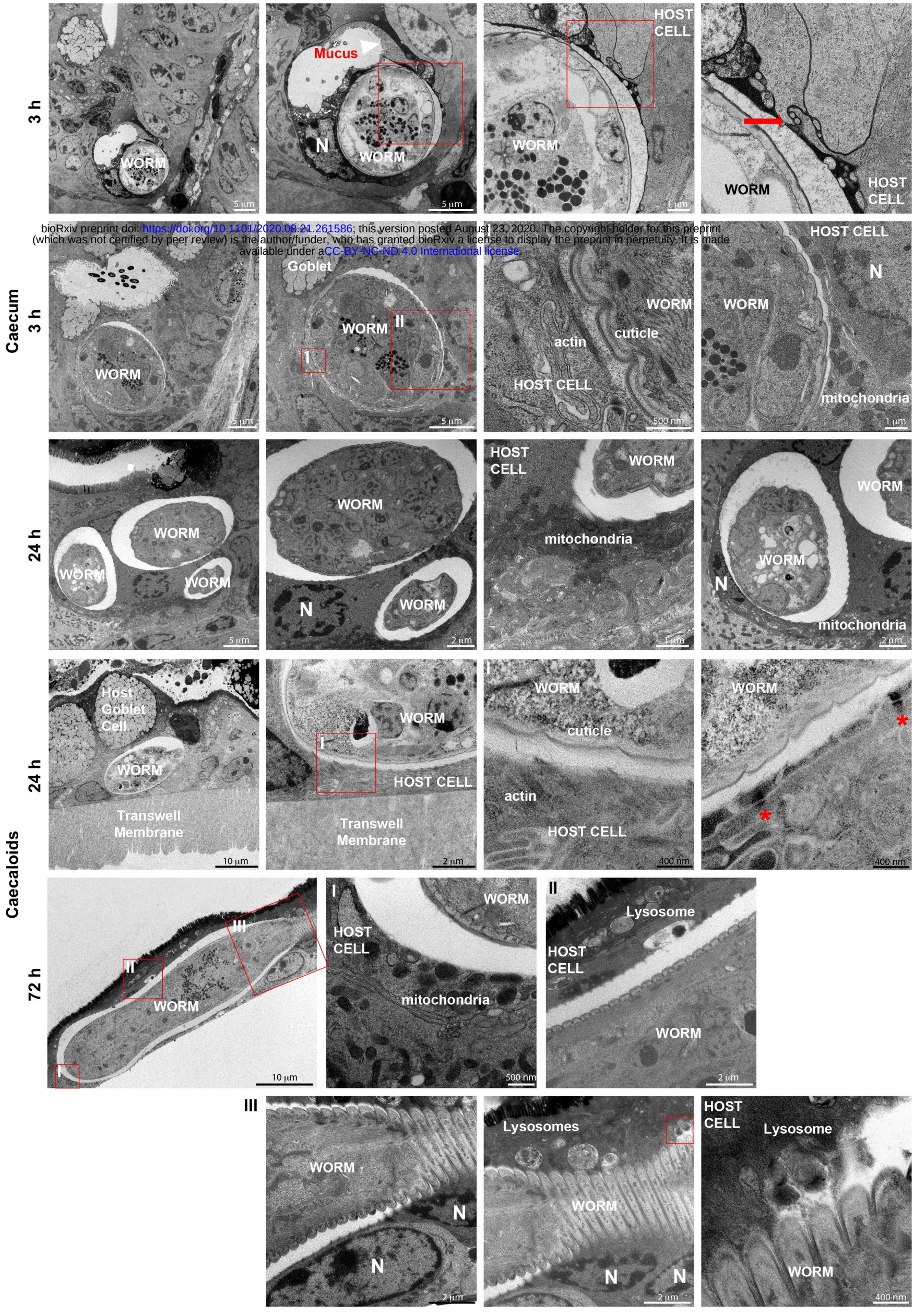

Figure 5.

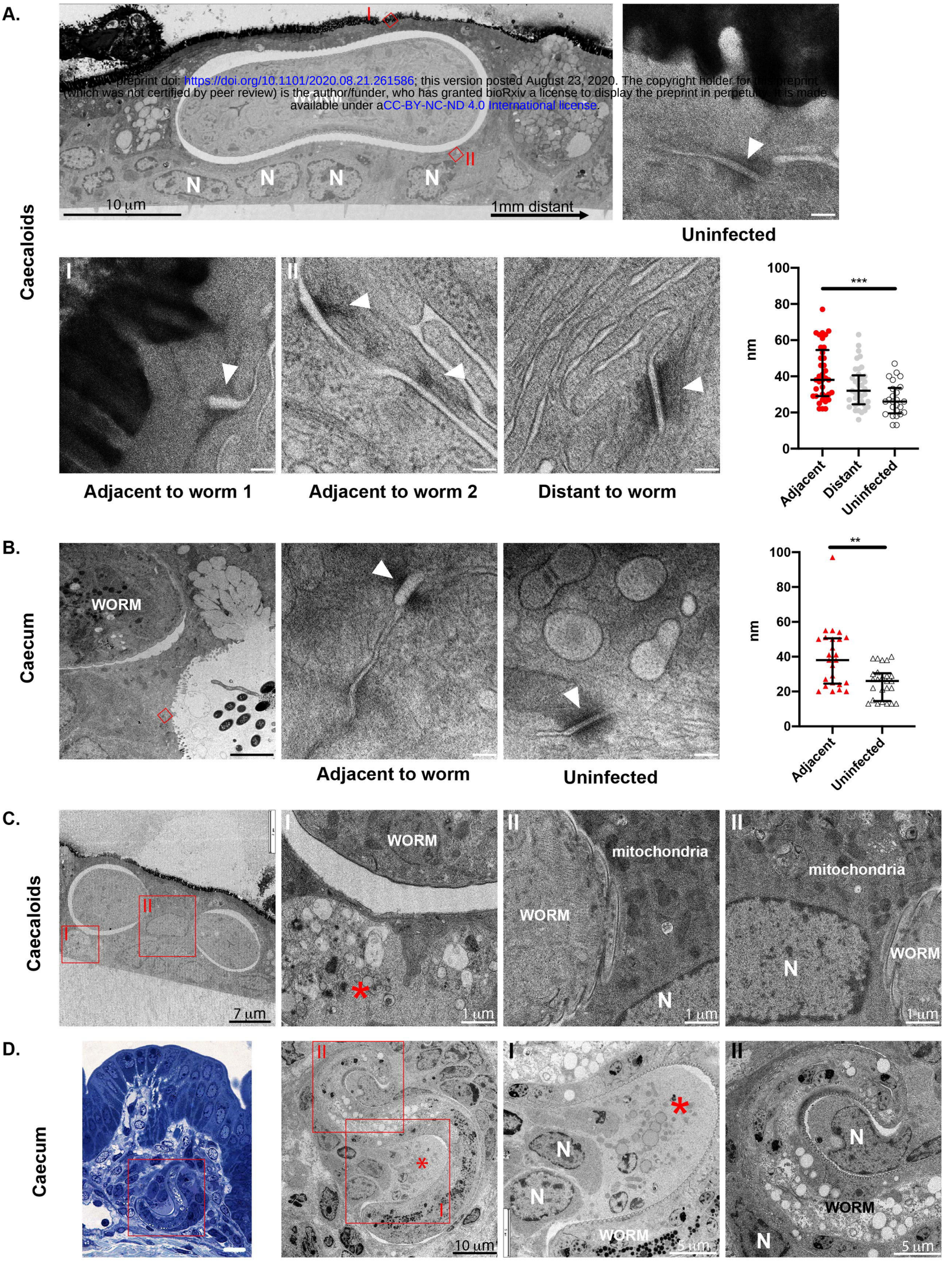

Supplementary Figure 1.

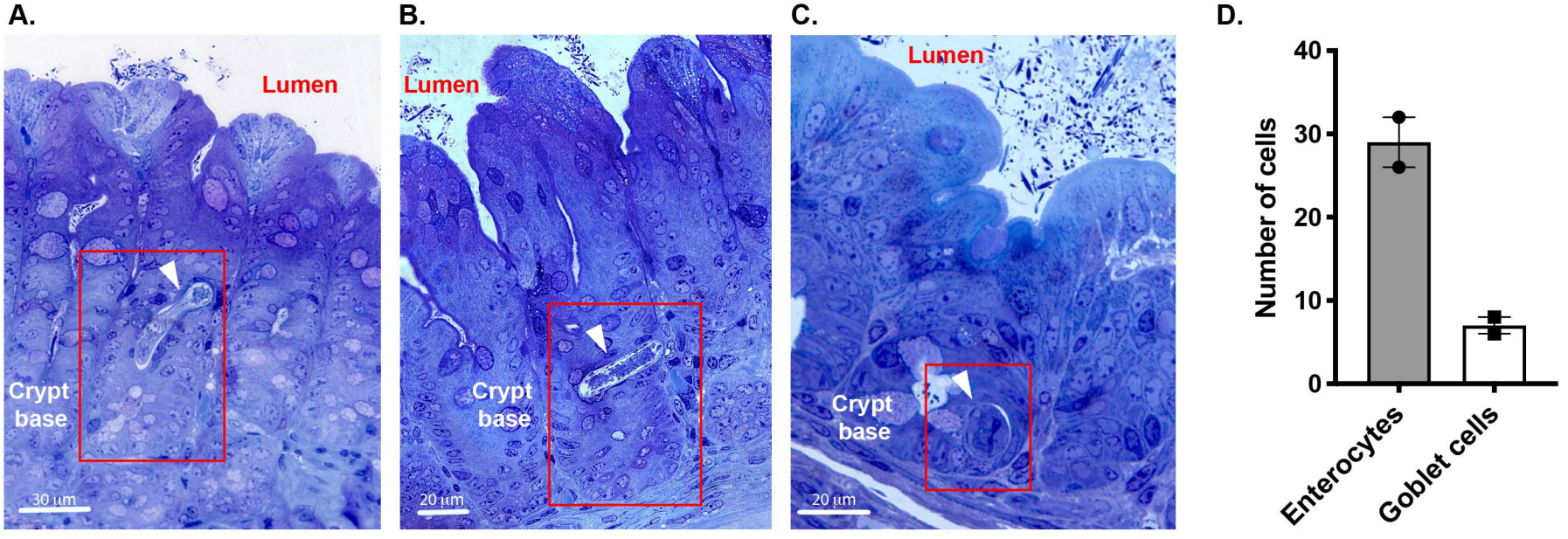

Supplementary Figure 2.

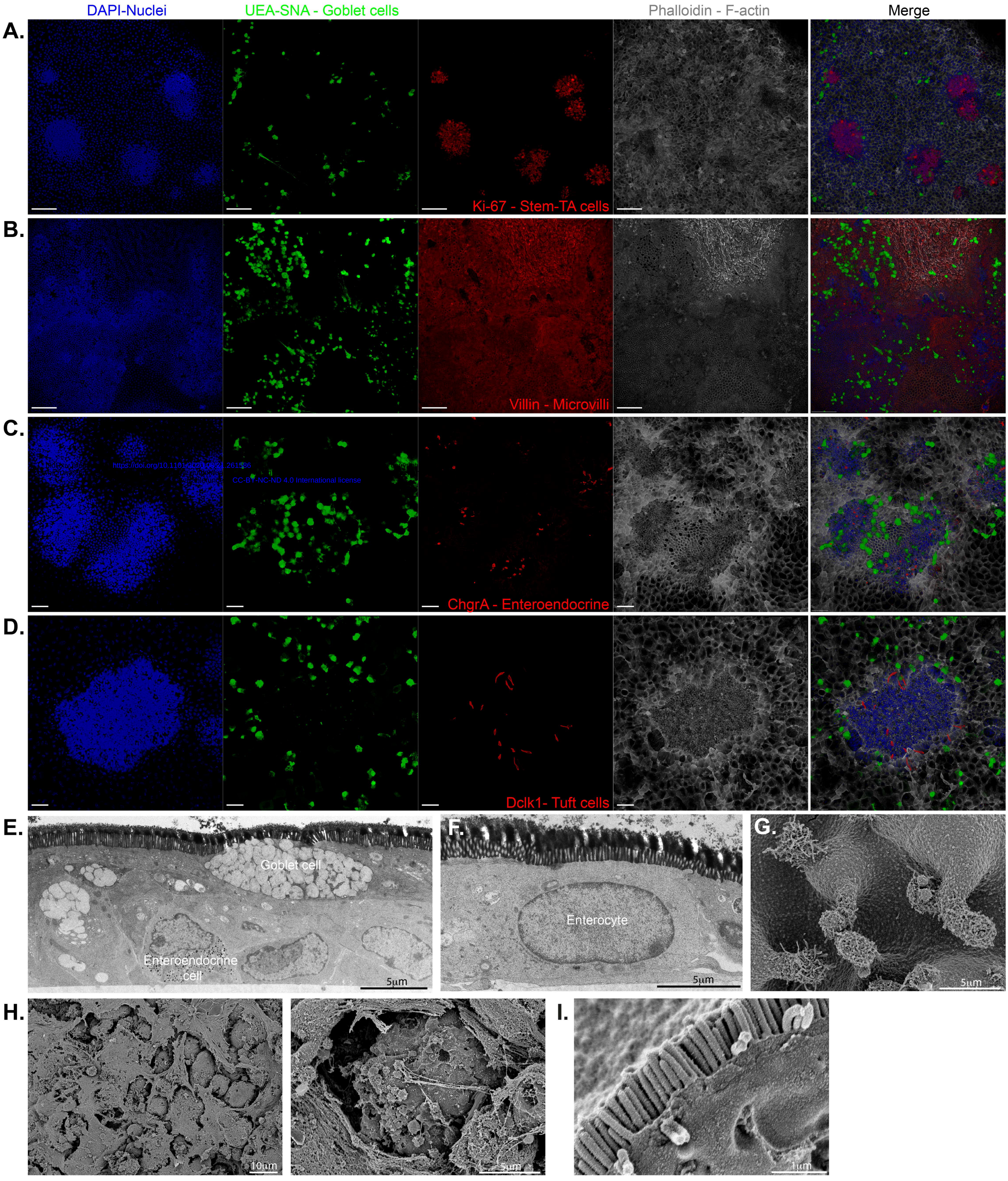

Supplementary Figure 3.